Supplementary Materials

Efficient catalysts for oxygen evolution reaction of five novel MOFs with various dimensions

Zhu-Meng Ren,[a] Lu-Lu Wang,[a] Jin-Miao Wang,[a] Bin Zhu,[a] Qiang Gao,[a] Mei Wang,[a] Feng Shao,*[a,b] and Yu-Hua Fan*[a]

[a]Key Laboratory of Marine Chemistry Theory and Technology, Ministry of Education, College of Chemistry and Chemical Engineering, Ocean University of China, Qingdao, Shandong 266100, China

[b]State Key Laboratory of Physical Chemistry of Solid Surfaces, College of Chemistry and Chemical Engineering, Xiamen University, Xiamen 361005, China

*Corresponding author. Email: feng.shao@ouc.edu.cn

fanyuhua301@163.com

Section S1: Pertinent crystallographic parameters

Table. S1 Crystallographic parameters for **1**–**5**.

Compound	**1**	**2**	**3**	**4**	**5**
Formula	$C_{23}H_{15}CoN_3O_5$	$C_{23}H_{15}NiN_3O_5$	$C_{27}H_{22}MnN_4O_5$	$C_{26}H_{20}MnN_4O_5$	$C_{46}H_{36}Mn_2N_6O_{13}$
Formula weight	472.31	472.09	537.42	523.40	990.69
Crystal system	Monoclinic	Monoclinic	Triclinic	Triclinic	Triclinic
Space group	$P2_1/n$	$P2_1/n$	$P\bar{1}$	$P\bar{1}$	$P\bar{1}$
a (Å)	13.0834(4)	13.1164(4)	9.2544(5)	9.3110(9)	10.0622(5)
b (Å)	16.1875(6)	16.1174(5)	10.3343(6)	10.2559(9)	10.4320(5)
c (Å)	14.8675(4)	14.7873(5)	14.8355(8)	14.8910(14)	11.9877(6)
α (°)	90	90	105.384(2)	105.346(3)	67.814(2)
β (°)	109.440(1)	109.782(1)	93.551(2)	94.240(3)	71.390(2)
γ (°)	90	90	116.082(2)	115.645(3)	68.516(1)
V (Å^3)	2969.24(16)	2941.59(16)	1202.28(12)	1206.8(2)	1060.07(9)
Z	4	4	2	2	1
D_x (Mg^{-3})	1.057	1.066	1.485	1.440	1.552
m (mm^{-1})	0.61	0.69	0.60	0.59	0.67
Reflections collected	6203	5883	4900	4922	4292
Data / parameters	294	290	337	327	319
F (000)	964	968	554	538	508
Temperature (K)	170	150	170	150	170
R_{int}	0.073	0.077	0.055	0.076	0.046
$R[F^2 > 2s(F^2)]$	0.058	0.063	0.054	0.052	0.040
$wR(F^2)$	0.175	0.172	0.143	0.140	0.102

Table. S2 Selected bond lengths (Å) and bond angles (º) of **1**.

bond lengths (Å)		**bond angles (º)**	
Co1—O2	2.032(2)	O2—Co1—O5^{i}	107.43(10)
Co1—O5^{i}	2.215(2)	O2—Co1—O4^{i}	167.88(10)
Co1—O4^{i}	2.156(3)	O4^{i}—Co1—O1	88.50(11)
Co1—O1	2.103(3)	N3^{ii}—Co1—O5^{i}	152.97(11)
Co1—N3^{ii}	2.103(3)	N3^{ii}—Co1—N1^{iii}	95.80(12)
Co1—N1^{iii}	2.147(3)	O2—Co1—O1	89.30(10)
		O4^{i}—Co1—N1^{iii}	93.25(11)
		O2—Co1—N1^{iii}	87.80(11)
		N1^{iii}—Co1—O1	174.02(11)
		O1—Co1—O5^{i}	84.79(10)
		O4^{i}—Co1—O5^{i}	60.50(9)
		N3^{ii}—Co1—O4^{i}	92.96(11)
		N3^{ii}—Co1—O1	89.81(11)
		N1^{iii}—Co1—O5^{i}	91.10(11)
		O2—Co1—N3^{ii}	98.95(11)

Symmetry codes: (i) *x*-1/2, -*y*+1/2, *z*-1/2; (ii) *x*, *y*, *z*-1; (iii) -*x*+3/2, *y*-1/2, -*z*+3/2; (iv) *x*+1/2, -*y*+1/2, *z*+1/2; (v) *x*, *y*, *z*+1; (vi) -*x*+3/2, *y*+1/2, -*z*+3/2.

Table. S3 Selected bond lengths (Å) and bond angles (º) of **2**.

bond lengths (Å)		**bond angles (º)**	
Ni1—O3	2.027(3)	O3—Ni1—O5^{i}	106.06(11)
Ni1—O5^{i}	2.195(3)	O3—Ni1—O4^{i}	167.89(12)
Ni1—O4^{i}	2.087(3)	O3—Ni1—O1	89.62(11)
Ni1—O1	2.107(3)	O3—Ni1—N3^{ii}	87.60(12)
Ni1—N3^{ii}	2.090(3)	O3—Ni1—N2^{iii}	97.19(13)
Ni1—N2^{iii}	2.050(4)	O4^{i}—Ni1—O5^{i}	61.84(11)
		N2^{iii}—Ni1—O4^{i}	94.82(12)
		N2^{iii}—Ni1—N3^{ii}	95.57(14)
		O4^{i}—Ni1—O1	88.96(12)
		O4^{i}—Ni1—N3^{ii}	92.77(12)
		O1—Ni1—O5^{i}	85.63(11)
		N3^{ii}—Ni1—O5^{ii}	90.59(12)
		N3^{ii}—Ni1—O1	174.50(13)
		N2^{iii}—Ni1—O5^{i}	156.18(12)
		N2^{iii}—Ni1—O1	89.48(13)

Symmetry codes: (i) x+1/2, -y+3/2, z+1/2; (ii) -x+1/2, y+1/2, -z+1/2; (iii) x, y, z+1; (iv) x-1/2, -y+3/2, z-1/2; (v) -x+1/2, y-1/2, -z+1/2; (vi) x, y, z-1.

Table. S4 Selected bond lengths (Å) and bond angles (º) of **3**.

bond lengths (Å)		**bond angles (º)**	
Mn01—O3^{i}	2.122(2)	O3^{i}—Mn01—O2	101.20(9)
Mn01—O2	2.122(2)	O3^{i}—Mn01—O4^{ii}	92.98(9)
Mn01—O4^{ii}	2.296(2)	O3^{i}—Mn01—O5^{ii}	93.96(9)
Mn01—O5^{ii}	2.235(2)	O3^{i}—Mn01—O1	86.88(10)
Mn01—O1	2.129(3)	O3^{i}—Mn01—N1^{iii}	174.66(10)
Mn01—N1^{iii}	2.343(3)	O2—Mn01—O4^{ii}	155.38(9)
		O2—Mn01—O5^{ii}	100.56(9)
		O2—Mn01—O1	112.18(11)
		O2—Mn01—N1^{iii}	83.31(9)
		O4^{ii}—Mn01—N1^{iii}	83.80(9)
		O5^{ii}—Mn01—O4^{ii}	58.07(9)
		O5^{ii}—Mn01—N1^{iii}	87.95(10)
		O1—Mn01—O4^{ii}	88.40(10)
		O1—Mn01—O5^{ii}	146.47(11)
		O1—Mn01—N1^{iii}	88.78(11)

Symmetry codes: (i) -x+1, -y+2, -z+2; (ii) x, y+1, z; (iii) -x+1, -y+1, -z+1; (iv) x, y-1, z.

Table. S5 Selected bond lengths (Å) and bond angles (º) of **4**.

bond lengths (Å)		**bond angles (º)**	
Mn01—O3	2.120(2)	O3—Mn01—O4^{i}	98.91(9)
Mn01—O4^{i}	2.139(2)	O3—Mn01—O1^{ii}	97.23(9)
Mn01—O1^{ii}	2.226(2)	O3—Mn01—O2^{ii}	153.49(9)
Mn01—O2^{ii}	2.278(2)	O3—Mn01—O5	108.90(10)
Mn01—O5	2.137(3)	O3—Mn01—N3^{iii}	84.10(9)
Mn01—N3^{iii}	2.315(3)	O4^{i}—Mn01—O1^{ii}	92.48(9)
		O4^{i}—Mn01—O2^{ii}	93.45(9)
		O4^{i}—Mn01—N3^{iii}	176.87(10)
		O1^{ii}—Mn01—O2^{ii}	58.67(8)
		O1^{ii}—Mn01—N3^{iii}	87.95(10)
		O2^{ii}—Mn01—N3^{iii}	84.13(9)
		O5—Mn01—O4^{i}	93.44(10)
		O5—Mn01—O1^{ii}	151.92(10)
		O5—Mn01—O2^{ii}	93.56(10)
		O5—Mn01—N3^{iii}	84.77(11)

Symmetry codes: (i) -x+1, -y+2, -z+2; (ii) x, y+1, z; (iii) -x+1, -y+1, -z+1; (iv) x, y-1, z.

Table. S6 Selected bond lengths (Å) and bond angles (º) of **5**.

bond lengths (Å)		**bond angles (º)**	
Mn01—O1^{i}	2.2224(17)	O1^{i}—Mn01—O3^{i}	57.35(6)
Mn01—O6	2.1661(18)	O1^{i}—Mn01—N3^{ii}	94.15(8)
Mn01—O5	2.2130(19)	O6—Mn01—O1^{i}	146.64(7)
Mn01—O3^{i}	2.3549(17)	O6—Mn01—O5	92.47(7)
Mn01—O4	2.1722(17)	O6—Mn01—O3^{i}	89.61(7)
Mn01—N3^{ii}	2.274(2)	O6—Mn01—O4	128.46(8)
		O6—Mn01—N3^{ii}	89.94(8)
		O5—Mn01—O1^{i}	172.25(7)
		O4—Mn01—O1^{i}	84.86(7)
		O4—Mn01—O5	85.98(7)
		O4—Mn01—O3^{i}	141.74(7)
		O4—Mn01—N3^{ii}	86.76(7)
		N3^{ii}—Mn01—O3^{i}	90.00(7)
		O5—Mn01—O3^{i}	97.38(7)
		O5—Mn01—O1^{i}	87.89(7)

Symmetry codes: (i) x+1, y, z; (ii) -x+1, -y+2, -z+1; (iii) x-1, y, z.

Section S2: Thermogravimetric analyses and IR spectra

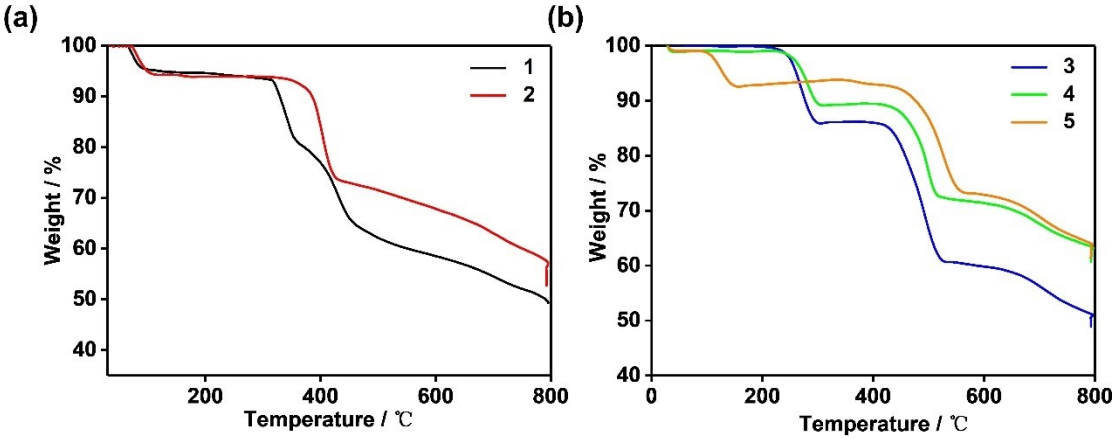

Fig. S1 Thermogravimetric analyses of **1**–**2** (a) and **3**–**5** (b). The TG curves indicated that **1**–**5** exhibited high thermal stability.

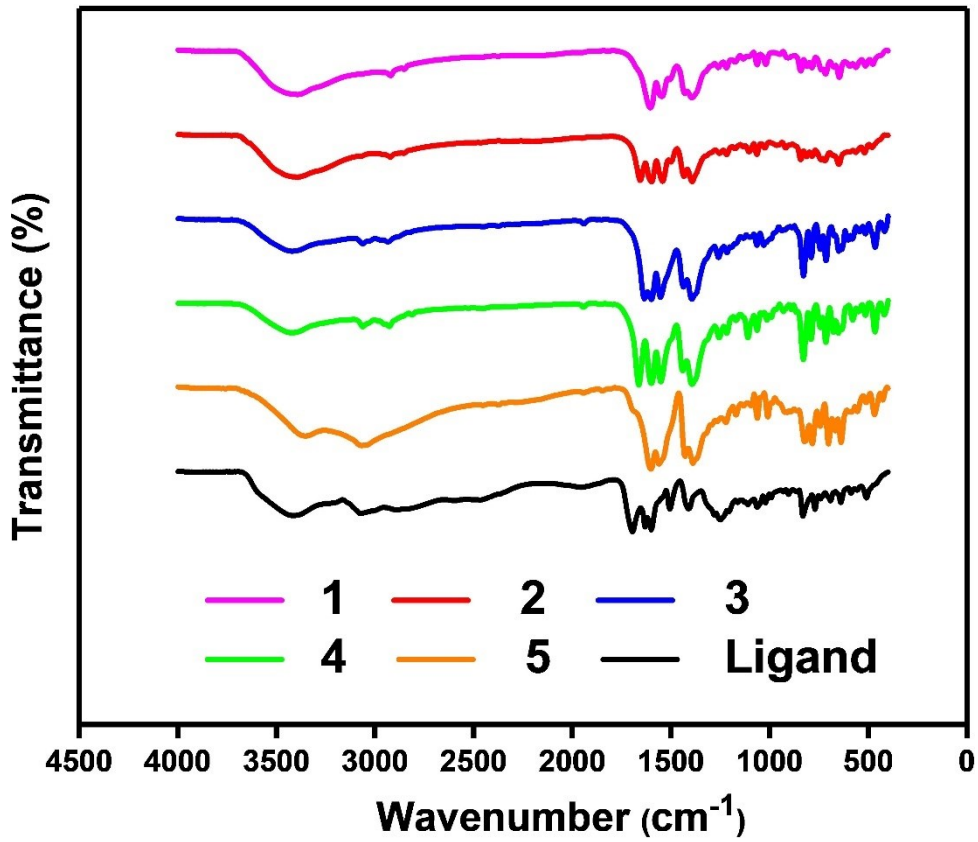

Fig. S2 IR spectra for the ligand and **1**–**5**. It revealed the structural integrity of **1**–**5**.

Section S3: Electrochemical Water Oxidation

The electrochemical studies were carried out in a single-chamber three-electrode electrolytic cell with CHI660E electrochemical analyser. In which the platinum wire electrode was used as counter electrode and Ag/AgCl was used as the reference electrode. The F-doped tin oxide (FTO) conducting glass substrates (1 cm × 1 cm, active surface area was 1.0 cm^2) acts as the working electrode. The observed potential values were converted to the reference of RHE by using the following equation.

$$E(\text{RHE}) = E(\text{Ag/AgCl}) + 0.0591*\text{pH} + 0.197$$

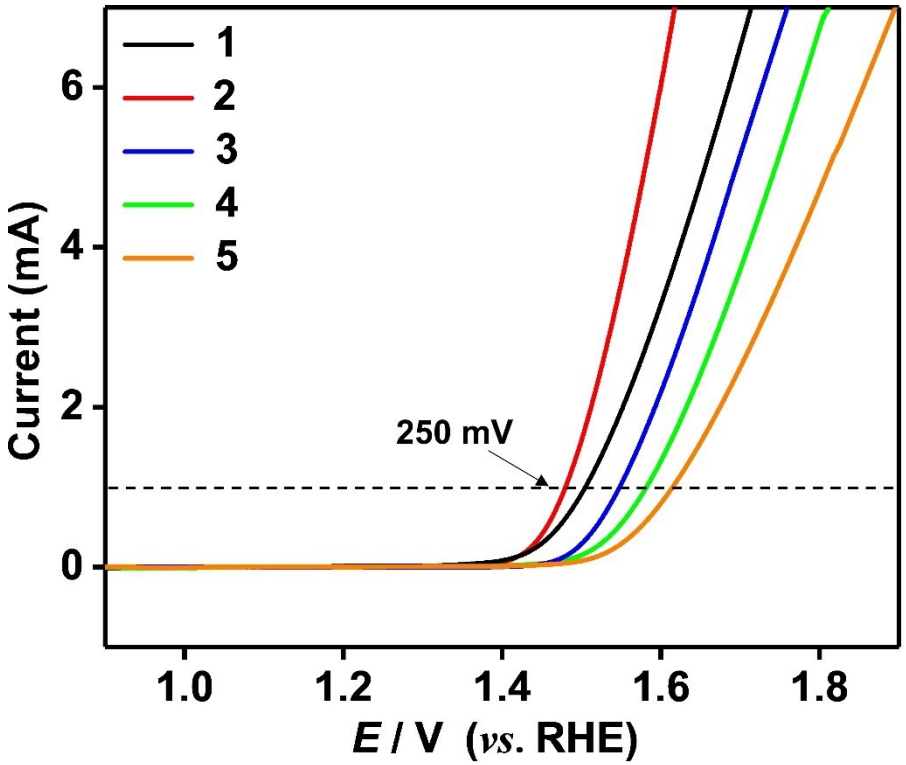

Fig. S3 Linear sweep voltammetry study for **1**–**5** after annealed (the samples of 1–5 was transferred to tubular furnace for annealing at 300 ℃ under Ar_2 for 1 h after drying in vacuum oven for 12 h.). The linear sweep voltammetry study of **1**–**5** after annealed has been collected. Under the same condition to generate the anode current density of 1 mA cm^{-2}, the overpotential can be obtained: 250, 280, 320, 350, 400 mV for the annealed samples of **1**–**5** respectively. The annealed samples of **1**–**5** lost the coordination water and solvent molecules in the skeleton after annealed which caused more higher overpotential. These results showed that the electrocatalytic performance of **1**–**5** after annealed has been decreased.

Section S3a: Cyclic voltammetry of 1–5.

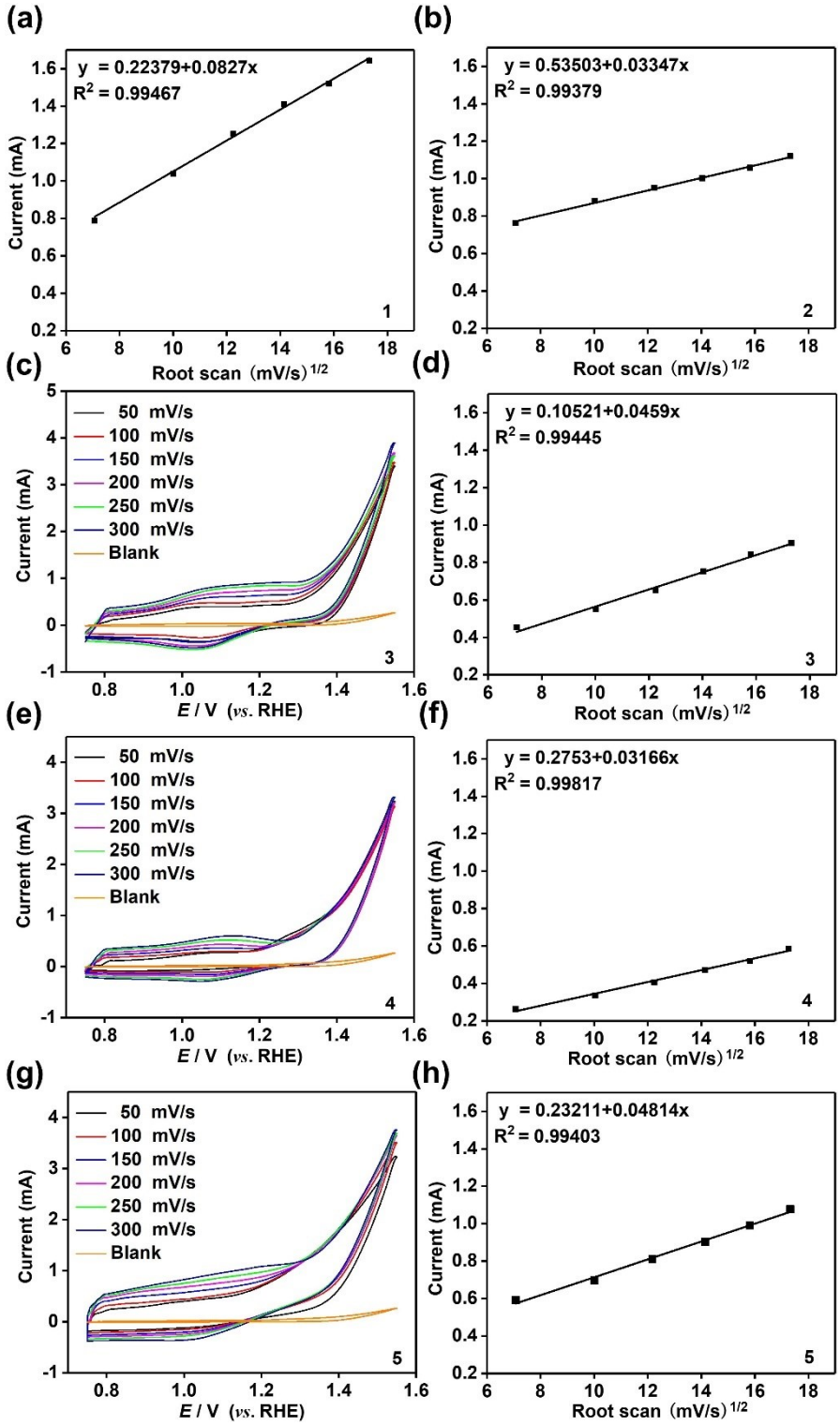

Fig. S4 CVs at various scan rates (50–300 mV/s) in Faradaic region for **3** (c), **4** (e), **5** (g). Dependence of peak current on scan rate for **1** (a), **2** (b), **3** (d), **4** (f), **5** (h). The peak current density of the electron transfer process was proportional to the square root of the scanning rate, which strongly demonstrated that the electrochemical process was diffusion controlled.

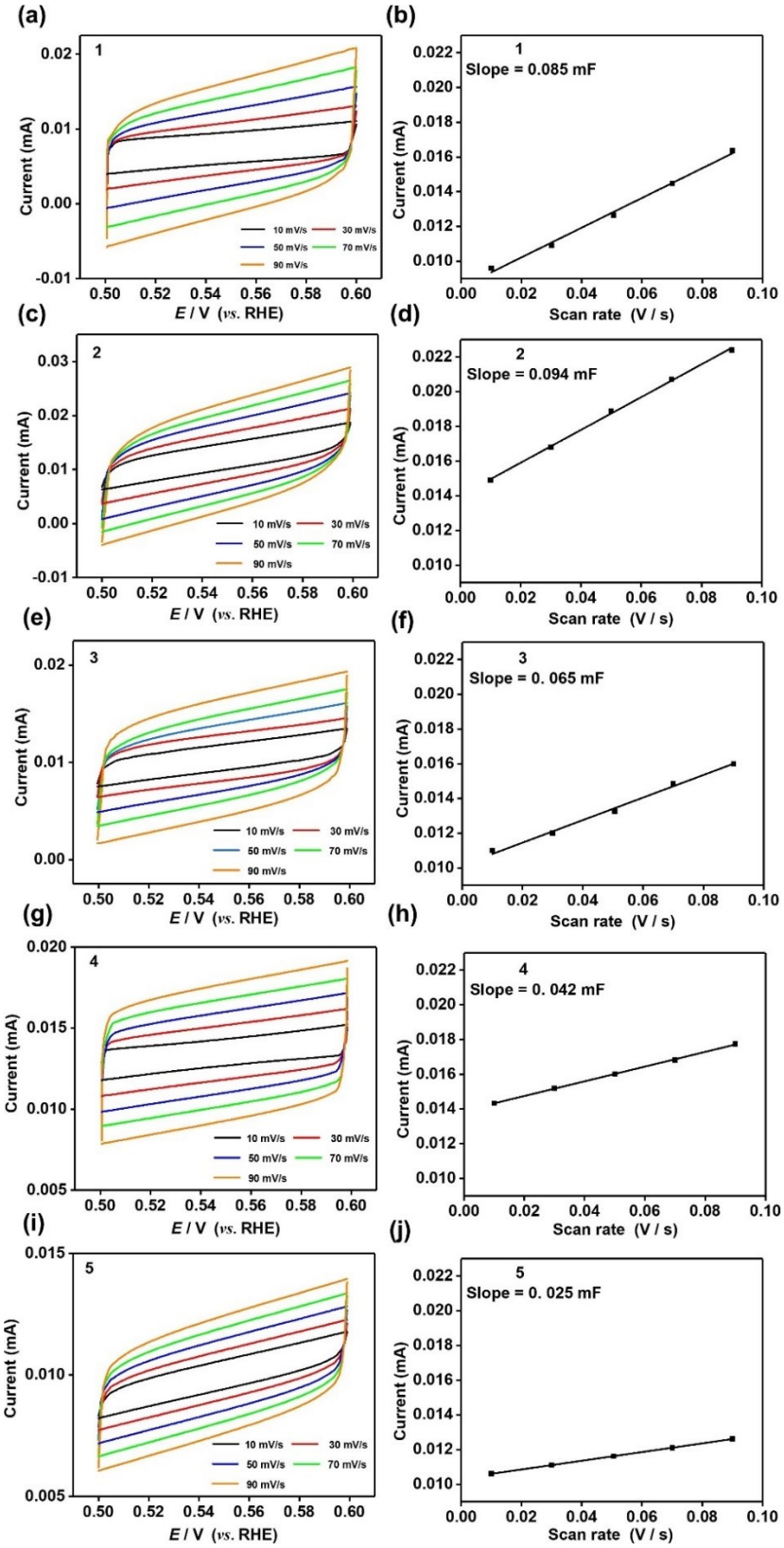

Fig. S5 Plot of CVs at various scan rates (10–90 mV/s) in the non-Faradaic region for **1** (a), **2** (c), **3** (e), **4** (g), **5** (i). Plot of capacitive current as a function of scan rate in the non-faradaic region for **1** (b), **2** (d), **3** (f), **4** (h), **5** (j). The linear slope was used to estimate the electrochemical double-layer capacitances C_{dl}.

Section S3b: Electrochemical assessable surface area (EASA)

The EASA of MOF catalysts can be calculated by the following formula:

$$\mathbf{EASA = C_{dl}/C_s}$$

$\mathbf{C_{dl}}$ (electrochemical double layer capacitance): By measuring the CVs at various scan rates (10 to 90 mV/s) in the non-faradaic region. The slope of the plot of capacitive current as a function of scan rate in the non-faradaic region (Fig. S5) is the value of C_{dl} for the MOF catalysts.

$\mathbf{C_s}$ (electrochemical double layer capacitance): In this paper, specific electrochemical double layer capacitance of an atomically smooth surface (C_s) had been taken 15 μF cm^{-2}. The EASA values of the five MOF catalysts have been listed in Table S7.

Section S3c: Roughness Factor (R_f)

The roughness factor of MOF catalysts can be calculated by the following formula:

$$\boldsymbol{R_f}\mathbf{ = EASA/geometrical\ area\ of\ the\ working\ electrode.}$$

Here, the geometrical surface area of the working electrode is 1 cm^2. Table S7 lists the R_f values obtained for the five MOF catalysts.

Section S3d: Turn Over Frequency (TOF)

The TOF of MOF catalysts can be calculated by the following formula:

$$\mathbf{TOF} = \boldsymbol{j} \times \boldsymbol{A}/(\mathbf{4} \times \boldsymbol{F} \times \boldsymbol{N_s})$$

where j is the current density (A cm^{-2}) at a given overpotential, A is the area of the electrode (cm^2), F is the Faraday constant (96485 C mol^{-1}), and N_s expresses the concentration of active sites in the catalysts (mol cm^{-2}).

Table. S7 OER performance for **1**–**5**.

Compound	Overpotential (mV)	Tafel Slope (mV/decade)	EASA (cm^2)	Roughness factor (R_f)	TOF (s^{-1})
1	130	70	5.7	5.7	0.67
2	110	64	6.3	6.3	0.74
3	260	92	4.3	4.3	0.34
4	290	95	2.8	2.8	0.26
5	330	105	1.7	1.7	0.31

Note: Comparison of the OER activities of **1**–**5** in this work. Among all the data above, it indicated that **2** showed very competitive OER performance between **1**–**5**.

Section S4: The possible mechanism for OER in alkaline medium

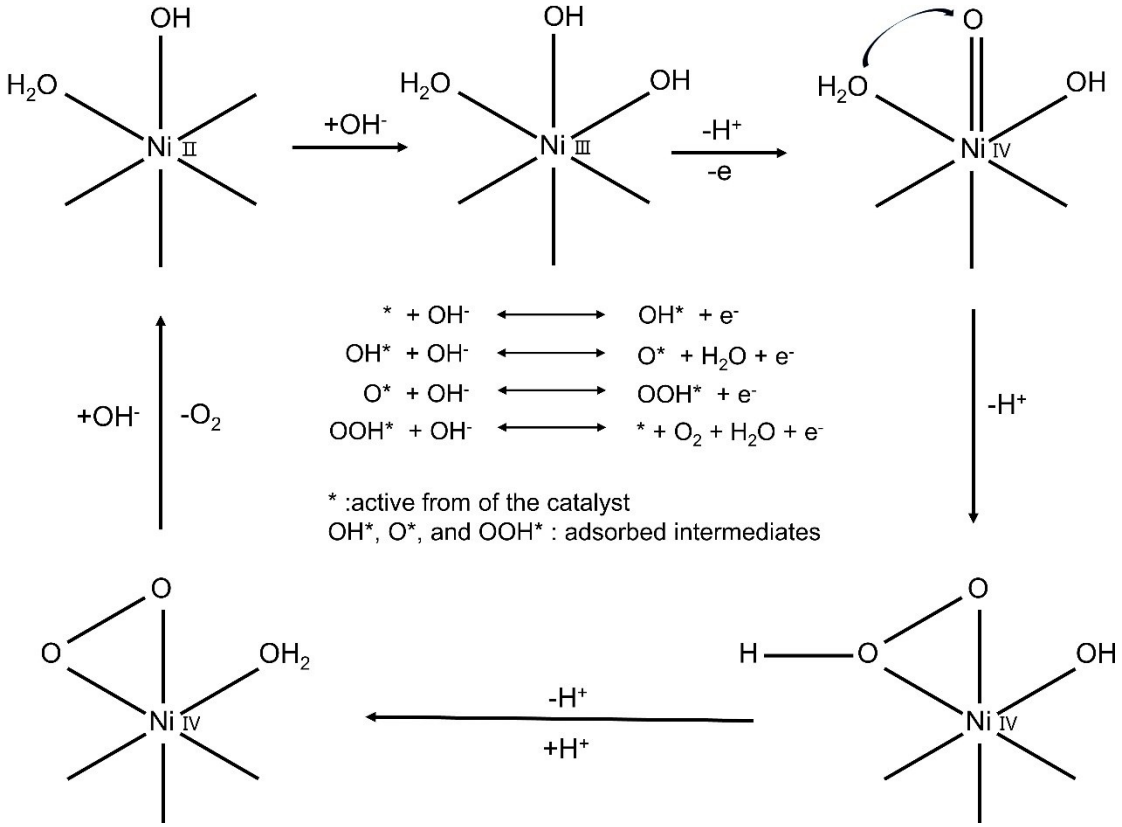

Fig. S6 The possible mechanism for OER in alkaline medium with Ni^{2+}/Ni^{3+} for **2**. The simultaneously coupled electron and proton transfer processes by the MOF oxidize the Ni^{II} centres to Ni^{III} and subsequently to Ni^{IV} and then reduce to Ni^{II} by releasing one mole of O_2.

Section S5: PXRD patterns of the 1–5

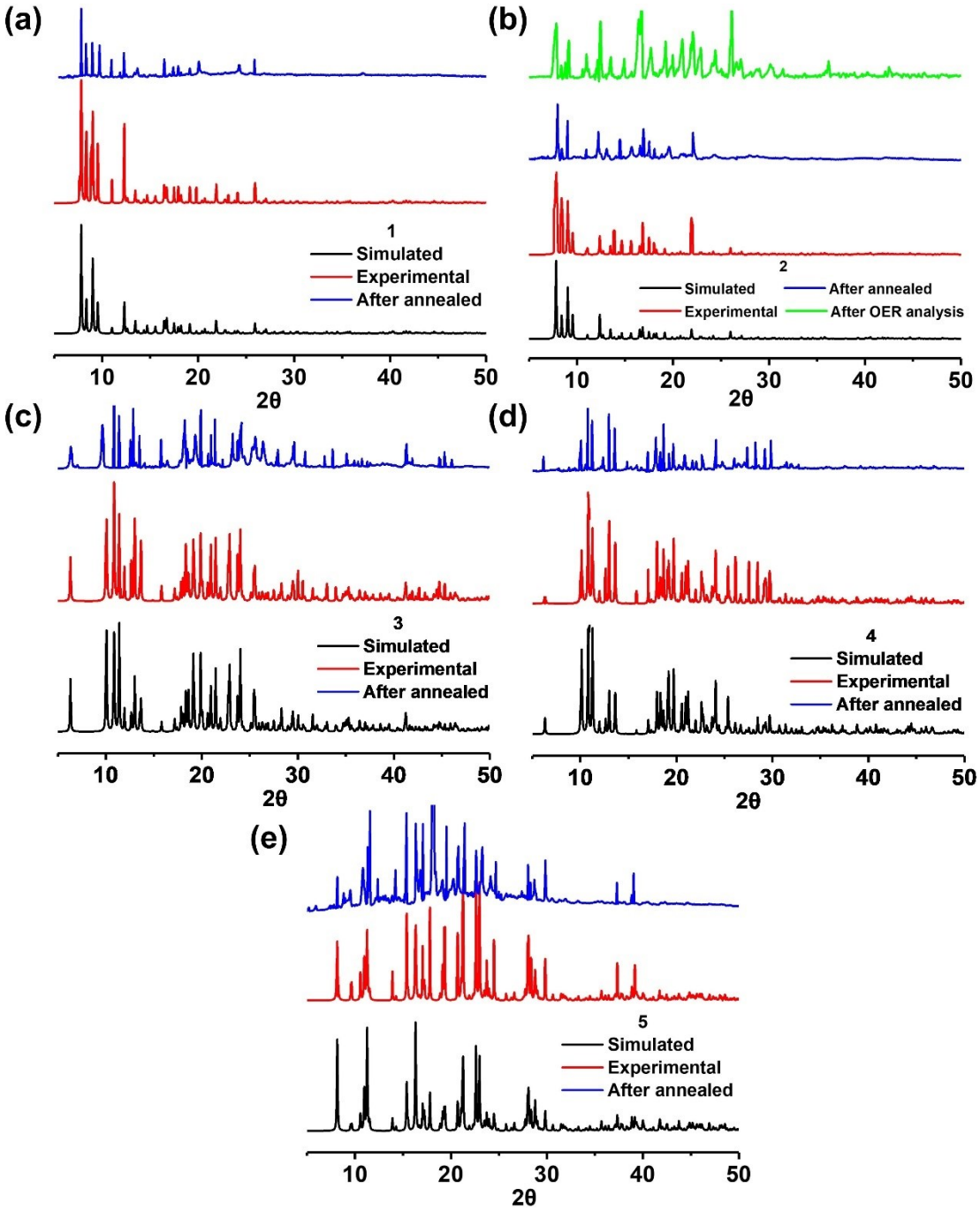

Fig. S7 PXRD pattern for **1** (a), **2** (b), **3** (c), **4** (d), **5** (e). The PXRD data revealed the typical diffraction peaks of **1**–**5**, which confirmed the successful synthesis of the target products and proved the structural stability of **2** after OER analysis. The corresponding diffraction peaks of the **1**–**5** were mainly retained after annealed, which indicated the excellent stability of catalyst **1**–**5**.

Section S6: Comparison of OER performances

Table. S8 OER performance comparison of several MOFs recently reported as electrocatalysts.

Catalysts	Overpotential (mV)	Electrolyte	Ref
(Co-WOC-1) $\{Co(H_2O)_4(DMF)_2\}^{2+}$	390	0.1 M KOH	[1]
Co-Cd-BNN MOF	353	0.1 M KOH	[2]
NNU-23 (Fe_2Ni-MOF)	365	0.1 M KOH	[3]
Co-BDC nanosheets	371	0.1 M KOH	[4]
NiPc-MOF	390	0.1 M KOH	[5]
Co-MOF/NF	380	0.1 M KOH	[6]
UTSA-16	360	0.1 M KOH	[7]
MIL-101(Cr)	329	0.1 M KOH	[8]
NH_2TA-Ni-MOF	356	0.1 M KOH	[9]
$\{[Ni(L_2)_2(TA)]\cdot 4H_2O\}_n$	400	0.1 M KOH	[10]
FeCo-MNS-1.0	298	0.1 M KOH	[11]
3D-Ni/CoMOFs	264	0.1 M KOH	[12]
$[Co(dcpbpy)(H_2O)]_n$	170	0.1 M KOH	This work
$[Ni(dcpbpy)(H_2O)]_n$	130	0.1 M KOH	This work
$[Mn(dcpbpy)(DMAc)]_n$	270	0.1 M KOH	This work
$[Mn(dcpbpy)(DMF)]_n$	290	0.1 M KOH	This work
$[Mn(dcpbpy)(H_2O)_2]_n$	350	0.1 M KOH	This work

Note: Comparison of the OER activities of **1**–**5** in this work with some work recently-reported. Among the materials above, it shows the competitive OER performance in our work.

References:

1. P. Manna, J. Debgupta, S. Bose and S. K. Das, *Angew. Chem. Int. Ed.*, 2016, **55**, 2425-2430.
2. K. Maity, K. Bhunia, D. Pradhan and K. Biradha, *ACS Appl. Mater. Interfaces*, 2017, **9,** 37548-37553.
3. X. L. Wang, L. Z. Dong, M. Qiao, Y. J. Tang, J. Liu, Y. Li, S. L. Li, J. X. Su and Y. Q. Lan, *Angew. Chem. Int. Ed.*, 2018, **57**, 9660-9664.
4. S. Zhao, Y. Wang, J. Dong, C. T. He, H. Yin, P. An, K. Zhao, X. Zhang, C. Gao and L. Zhang, *Nat. Energy*, 2016, **1**, 1-10.
5. H. Jia, Y. Yao, J. Zhao, Y. Gao, Z. Luo and P. Du, *J. Mater. Chem. A*, 2018, **6**, 1188-1195.
6. X. Zhang, W. Sun, H. Du, R.-M. Kong and F. Qu, *Inorg. Chem. Front.*, 2018, **5**, 344-347.
7. J. Jiang, L. Huang, X. Liu and L. Ai, *ACS Appl. Mater. Interfaces*, 2017, **9**, 7193-7201.
8. B. Nepal and S. Das, *Angew. Chem. Int. Ed.*, 2013, **52**, 7224-7227.
9. S. K. Konavarapu, D. Ghosh, A. Dey, D. Pradhan and K. Biradha, *Chem. - Eur. J.*, 2019, **25**, 11141-11146
10. A. Goswami, D. Ghosh, V. V. Chernyshev, A. Dey, D. Pradhan and K. Biradha, *ACS Appl. Mater. Interfaces*, 2020, **12**, 33679-33689.
11. L. Zhuang, L. Ge, H. Liu, Z. Jiang, Y. Jia, Z. Li, D. Yang, R. K. Hocking, M. Li, L. Zhang, X. Wang, X. Yao and Z. Zhu, *Angew. Chem. Int. Ed.*, 2019, **58**, 13565-13572.
12. P. Luo, S. Li, Y. Zhao, G. Ye, C. Wei, Y. Hu and C. Wei, *ChemCatChem*, 2019, **11**, 6061-6069.